Asymmetric solitons in coupled second-harmonic-generating waveguides

William C. K. Mak,[1,*] Boris A. Malomed,[2,†] and P. L. Chu[1,‡]
[1]*Optical Communications Group, School of Electrical Engineering, University of New South Wales, Kensington, New South Wales 2052, Australia*
[2]*Department of Interdisplinary Studies, Faculty of Engineering, Tel Aviv University, Tel Aviv 69978, Israel*
(Received 14 May 1997; revised manuscript received 13 August 1997)

We report results of analytical and numerical consideration of solitons in a system of two linearly coupled second-harmonic-generating waveguides. We consider the system with arbitrary coupling constants for the fundamental and second harmonics, and with an arbitrary (but equal) mismatch inside each waveguide (in a previous work, only the limit case of equal coupling constants, and a single value of the mismatch, were considered). Two regions of existence of nontrivial asymmetric soliton states, along with bifurcation lines at which they bifurcate from obvious symmetric solitons, are identified. The analytical approach is based on the variational approximation, which is followed by direct numerical solution of the stationary ordinary differential equations. The analytical and numerical results are found to be in fairly good agreement, except for a very narrow parametric region, where the second-harmonic component of the soliton is changing its sign, having a nonmonotonous shape. We further establish the stability of the asymmetric solitons, simulating the corresponding partial differential equations, and simultaneously show that the coexisting symmetric solitons are unstable. We then analyze in detail the effects of a walkoff (spatial misalignment) between the two cores. We demonstrate that the asymmetric solitons remain stable if walkoff is small. When the walkoff becomes larger, the solitons get strongly distorted, and finally destruct when walkoff gets too large. [S1063-651X(97)05912-6]

PACS number(s): 42.65.Tg

I. INTRODUCTION

The study of waveguides with quadratic nonlinearities began more than two decades ago [1]. The solitons in such waveguides have, however, attracted a lot of attention only recently [2,3]. Coupling effects in systems of this type were dealt with in a few works [4,5]; nevertheless, solitary-wave states were not considered there. In a recent work, solitons in a model of parallel-coupled waveguides with quadratic (second-harmonic-generating) nonlinearity were studied by the present authors [6]. The solitons in this system share some qualitative properties with the ones previously studied in detail in models of nonlinear dual-core optical fibers with the cubic (Kerr) nonlinearity, see, e.g., [7] and [8]. A bifurcation that transforms obvious symmetric solitons in the coupled quadratically nonlinear waveguides into nontrivial asymmetric solitons has been found in [6]. The asymmetric states were shown to be stable, while the coexisting symmetric solitons were unstable. A drastic difference from the symmetry-breaking bifurcation in the dual-core fibers with the Kerr nonlinearity, where the bifurcation is subcritical, is the fact that, in the parallel-coupled second-harmonic-generating waveguides, the bifurcation is supercritical.

However, in Ref. [6], only a very limited situation was considered, the most essential limitation being the assumption of equal coupling constants between the fundamental harmonics (FH) and between the second harmonics (SH). Additionally, a single special value of the mismatch parameter between the two harmonics inside each waveguide was dealt with (the one at which the single waveguide has an exact analytical solution [1]). Both these assumptions are, evidently, very restrictive; in particular, the former one implies a very small separation between the waveguides. Moreover, consideration of the general case of unequal couplings is of principal interest because it has no analog in terms of the single waveguide [2,3].

The aim of the present work is to extend the study of the solitons in parallel-coupled quadratically nonlinear waveguides, removing the assumption of equal coupling coefficients, and also varying the mismatch parameter. We will denote the FH and SH coupling constants as Q and K, respectively. The main issues to be considered are the asymmetric solitons and bifurcations that give rise to them, stability of the asymmetric and symmetric solitons, and walkoff effects.

The exact location of the point of the bifurcation that gives rise to asymmetric solitons found in [6] for the limit case $K=Q$ and for the single value of the mismatch was at $Q=5/13$. In the present work, it will be shown that the bifurcation point moves, depending on the value of Q/K. It may be located anywhere between $K=5/13$ and $K=-1$. Outside this range, the bifurcation does not occur, hence only the obvious symmetric solitons exist.

In the generic case, with different coupling coefficients and for different values of the mismatch parameter, we will demonstrate that general conclusions on stability of the soliton states are in line with those in [6]: the bifurcation is supercritical, with the asymmetric states stable and the coexisting symmetric ones unstable. Moreover, we will also show that the asymmetric states remain stable when a misalignment between the two beams, producing a spatial walkoff, is added to the model, provided that this misalignment is not too large. When the misalignment becomes too large, the

*Electronic address: w.mak@ee.unsw.edu.au
†Electronic address: malomed@eng.tau.ac.il
‡Electronic address: p.chu@unsw.edu.au

solitons will finally destruct. We also interpret the characteristic values of the misalignment in terms of the corresponding angle between the beams in the two cores.

A general model to describe the copropagation of FH u and SH v in the linearly coupled waveguides was put forward in [6]:

$$iu_{1z}+i\delta u_{1x}+\frac{1}{2}u_{1xx}-qu_1+u_1^*v_1=-Qu_2, \tag{1}$$

$$2iv_{1z}+2i\delta v_{1x}+\frac{1}{2}v_{1xx}-v_1+\frac{1}{2}u_1^2=-Kv_2, \tag{2}$$

$$iu_{2z}-i\delta u_{2x}+\frac{1}{2}u_{2xx}-qu_2+u_2^*v_2=-Qu_1, \tag{3}$$

$$2iv_{2z}-2i\delta v_{2x}+\frac{1}{2}v_{2xx}-v_2+\frac{1}{2}u_2^2=-Kv_1, \tag{4}$$

where the subscripts 1 and 2 pertain to the first and second waveguides, z and x being, respectively, the propagation and transverse coordinates in them, and δ is the walkoff parameter. The second derivatives and the nonlinear terms in Eqs. (1)–(4) account for, respectively, diffraction and FH-SH conversion, while the terms on the right-hand sides represent the linear coupling between the waveguides. Lastly, the parameter q measures the phase mismatch between the two harmonics inside each core (individual waveguide). Note that the other frequently used mismatch parameter α, defined as a coefficient in the equation for SH [2], is q^{-1}. The usual definition of the full matching refers to $q=\frac{1}{4}$. However, the case most convenient for consideration is $q=1$, when the single-core model has the famous Karamzin-Sukhorukov analytical solution [1]. The terms on the right-hand sides represent the linear coupling between the waveguides.

In most of this work, the phase mismatch parameter q will be fixed at this ''convenient'' value, $q=1$. Thus, we can concentrate on the effects of changing the ratio Q/K, which corresponds, physically, to varying the separation between the two cores. In this part of the work, result will be formulated in the form of the three-dimensional bifurcations diagrams, which are a far-reaching extension of the simple diagram obtained in [6]. Then, arbitrary values of the mismatch will be considered (which was not done at all in [6]). A general conclusion is that, as q gets smaller than 1, the regions of the existence of the asymmetric soliton states shrink, while the opposite happens when $q>1$. As q increases, the asymmetry between the soliton components in the two cores increases rapidly. This leads to quite a natural conclusion that the two waveguides get decoupled as the phase mismatch increases.

In most of this work, we will deal with the no-walkoff case, $\delta=0$. However, at the end of the paper, effects produced by the walkoff will be considered too. Note that, for the limit case $K=Q$, the stability of the asymmetric soliton states against moderate walkoff has been established in [6]. In the present work, we will show, gradually increasing the value of δ in direct partial diferential equation (PDE) simulation, that the solitons get distorted, and finally destruct as δ gets too large.

To obtain stationary solutions, one should drop the z-derivative terms in Eqs. (1)–(4), and set all the variables real. In [6], the variational approximation (VA) was used to obtain an analytical approximation to the stationary solutions in the limit case $K=Q$. VA has produced approximate solutions with very good accuracy, when compared with numerical results obtained by means of the well-known shooting method. In this work, dealing with the general case, we will have to both generalize the corresponding VA (we will use the Gaussian ansatz in order to allow for different widths of all four components of the soliton) and use, instead of the shooting method, a modifed version of the method of lines (see, e.g., [9]), in order to obtain numerical stationary solutions to Eqs. (1)–(4). The reason to change the numerical technique is that it must now handle a system of *four* equations, while in the particular case considered in [6], the equal coupling coefficients made it possible to reduce the system to two equations. Hence, initial estimates, which are needed when using these numerical methods, have to be made on four variables, instead of just two for the particular case $K=Q$. The use of the shooting method, which requires a very good initial guess, has turned out to be very difficult, if not impossible, in this case. On the contrary, the method of lines allows even rather poor initial guesses. Moreover, in the process of this work, it was also found that the method of lines was more numerically stable, allowing one to find asymmetric solutions at more negative values of the coupling constants, where the shooting method used in [6] had failed. This resolves a problem encountered in [6]: premature termination of the bifurcation curves at $Q=K\approx-0.3$. We can now make sure that the termination was a numerical artifact, and the genuine bifurcation curves can be continued all the way along the path predicted by VA.

Thus, our present solution methods, both analytical and numerical, impose no technical restrictions on the values of the coupling constants K and Q in Eqs. (1)–(4). However, there is a physical limitation $|K|\leqslant|Q|$: it is very unlikely that the SH coupling can be stronger than the FH coupling. With regard to this restriction, the range $K>5/13$ was not considered, because only evident symmetric solutions exist there. In the negative K domain, we will limit our investigation to $K>-1$, which is another boundary for the existence of asymmetric solutions. As for the bifurcation points, at which the asymmetric soliton solutions set in, branching off from the obvious symmetric ones, it will be found that, as K decreases, the bifurcation occurs at increasing values of $|Q|$, Q ranging between -1 and 1.

Stability of both symmetric and asymmetric solitons will be investigated both in the linear approximation and by direct simulations of Eqs. (1)–(4), using the split-step Fourier method (also called the beam propagation method). As mentioned above, the asymmetric soliton solutions prove to be stable always when they exist, while the symmetric ones coexisting with them are always unstable.

The paper is organized as follows. In Sec. II, we briefly describe the basic analytical and numerical techniques that will be used for analysis of the model. In Sec. III, we display the results for the stationary soliton solutions, as obtained by means of VA and by direct numerical integration of the corresponding ODE's. In Sec. IV, we display results of the stability analysis for the asymmetric and symmetric solitons. In

Sec. V, we consider the walkoff effect and demonstrate that the asymmetric solitons remain robust when this effect is small. We will then demonstrate the distortion of the solitons as walkoff is increased. In all these sections the case $q=1$ is considered. Lastly, in Sec. VI we will show the effect of varying the phase mismatch q between the FH's and the SH's. Conclusions are formulated in Sec. VII.

II. THE MATHEMATICAL TECHNIQUES

Equations determining stationary solutions are obtained from Eqs. (1)–(4) by dropping the z-derivative (and the walkoff) terms:

$$\frac{1}{2}u_{1xx}-qu_1+u_1^*v_1+Qu_2=0, \tag{5}$$

$$\frac{1}{2}v_{1xx}-v_1+\frac{1}{2}u_1^2+Kv_2=0, \tag{6}$$

$$\frac{1}{2}u_{2xx}-qu_2+u_2^*v_2+Qu_1=0, \tag{7}$$

$$\frac{1}{2}v_{2xx}-v_2+\frac{1}{2}u_2^2+Kv_1=0. \tag{8}$$

The Lagrangian of the ordinary differential equations (ODE's) (5)–(8), $L=\int_{-\infty}^{+\infty}\mathcal{L}dx$, can be derived with the Lagrangian density

$$\mathcal{L}=-\frac{1}{4}[(u_1')^2+(u_2')^2+(v_1')^2+(v_2')^2]-\frac{1}{2}q(u_1^2+u_2^2)-\frac{1}{2}(v_1^2+v_2^2)+Qu_1u_2+Kv_1v_2+\frac{1}{2}u_1^2v_1+\frac{1}{2}u_2^2v_2, \tag{9}$$

where the prime stands for d/dx. To search for soliton solutions by means of VA, we should adopt an *ansatz*. Unlike the sech^2-based ansatz used in [6], here we will use the more versatile Gaussian ansatz, which admits different widths of different components of the soliton (this ansatz was earlier applied to description of solitons in the single-core quadratically nonlinear waveguide with a varying mismatch parameter in [3]):

$$u_{1,2}=A_{1,2}\exp\left(-\frac{1}{2}\alpha_{1,2}x^2\right), \tag{10}$$

$$v_{1,2}=B_{1,2}\exp\left(-\frac{1}{2}\beta_{1,2}x^2\right), \tag{11}$$

where $A_{1,2}$, $B_{1,2}$, $\alpha_{1,2}$, and $\beta_{1,2}$ are the amplitudes and widths of the FH and SH of the soliton solution sought for. The subscripts 1 and 2 pertain to the two cores.

Inserting Eqs. (10) and (11) into Eq. (9), we calculate the effective Lagrangian,

$$\frac{2}{\sqrt{\pi}}L\equiv\frac{2}{\sqrt{\pi}}\int_{-\infty}^{+\infty}\mathcal{L}dx=-\frac{1}{4}A_1^2\sqrt{\alpha_1}-\frac{1}{4}A_2^2\sqrt{\alpha_2}-\frac{1}{4}B_1^2\sqrt{\beta_1}-\frac{1}{4}B_2^2\sqrt{\beta_2}-qA_1^2\alpha_1^{-1/2}-qA_2^2\alpha_2^{-1/2}-B_1^2\beta_1^{-1/2}-B_2^2\beta_2^{-1/2}$$
$$+2A_1A_2Q\sqrt{\frac{2}{\alpha_1+\alpha_2}}+2B_1B_2K\sqrt{\frac{2}{\beta_1+\beta_2}}+A_1^2B_1\sqrt{\frac{2}{2\alpha_1+\beta_1}}+A_2^2B_2\sqrt{\frac{2}{2\alpha_2+\beta_2}}. \tag{12}$$

The variational equations are obtained by demanding the variations of the effective Lagrangian with respect to each of $A_{1,2}$, $B_{1,2}$, $\alpha_{1,2}$, and $\beta_{1,2}$ to be zero. Then, we obtain the following eight equations:

$$-\frac{1}{2}A_1\alpha_1^{1/2}-2qA_1\alpha_1^{-1/2}+2A_2Q\sqrt{\frac{2}{\alpha_1+\alpha_2}}+2A_1B_1\sqrt{\frac{2}{2\alpha_1+\beta_1}}=0, \tag{13}$$

$$-\frac{1}{2}A_2\alpha_2^{1/2}-2qA_2\alpha_2^{-1/2}+2A_1Q\sqrt{\frac{2}{\alpha_1+\alpha_2}}+2A_2B_2\sqrt{\frac{2}{2\alpha_2+\beta_2}}=0, \tag{14}$$

$$-\frac{1}{2}B_1\beta_1^{1/2}-2B_1\beta_1^{-1/2}+2B_2K\sqrt{\frac{2}{\beta_1+\beta_2}}+A_1^2\sqrt{\frac{2}{2\alpha_1+\beta_1}}=0, \tag{15}$$

$$-\frac{1}{2}B_2\beta_2^{1/2}-2B_2\beta_2^{-1/2}+2B_1K\sqrt{\frac{2}{\beta_1+\beta_2}}+A_2^2\sqrt{\frac{2}{2\alpha_2+\beta_2}}=0, \tag{16}$$

$$-\frac{1}{8}A_1^2\alpha_1^{-1/2}+\frac{1}{2}qA_1^2\alpha_1^{-3/2}-\sqrt{2}A_1A_2Q(\alpha_1+\alpha_2)^{-3/2}-\sqrt{2}A_1^2B_1(2\alpha_1+\beta_1)^{-3/2}=0, \tag{17}$$

$$-\frac{1}{8}A_2^2\alpha_2^{-1/2}+\frac{1}{2}qA_2^2\alpha_2^{-3/2}-\sqrt{2}A_1A_2Q(\alpha_1+\alpha_2)^{-3/2}-\sqrt{2}A_2^2B_2(2\alpha_2+\beta_2)^{-3/2}=0, \tag{18}$$

$$-\frac{1}{8}B_1^2\beta_1^{-1/2}+\frac{1}{2}B_1^2\beta_1^{-3/2}-\sqrt{2}B_1B_2K(\beta_1+\beta_2)^{-3/2}-\frac{\sqrt{2}}{2}A_1^2B_1(2\alpha_1+\beta_1)^{-3/2}=0, \tag{19}$$

$$-\frac{1}{8}B_2^2\beta_2^{-1/2}+\frac{1}{2}B_2^2\beta_2^{-3/2}-\sqrt{2}B_1B_2K(\beta_1+\beta_2)^{-3/2}-\frac{\sqrt{2}}{2}A_2^2B_2(2\alpha_2+\beta_2)^{-3/2}=0. \tag{20}$$

Because these algebraic equations cannot be solved analytically, we resort to the numerical Newton-Raphson method. This involves calculation of the Jacobian matrix by finding the partial derivatives of expressions on the left-hand sides of Eqs. (13)–(20) with respect to the eight unknowns, $A_{1,2}$, $B_{1,2}$, $\alpha_{1,2}$, and $\beta_{1,2}$. The Jacobian matrix is thus of dimension 8×8. We will not go into further technical details here, as the Newton-Raphson method is well known.

The next step is to obtain stationary numerical solutions of Eqs. (1)–(4) directly. We will do this by means of the method of lines. To make a partial discretization, we discretize the transverse space variable x. We replace the integration domain dm of x by a set of n points:

$$x_k=(k-1)h, \quad k=1,2,\ldots,n, \quad h\equiv\frac{dm}{n-1}. \tag{21}$$

Along each of the lines (x_k,z) for $z\geqslant 0$, we denote the values of u_1 by u_{1k} (and similarly for u_2 and v_1, v_2). Then, the finite-difference approximation is used for u_{xx}:

$$u_{xx}=\frac{u_{k-1}-2u_k+u_{k+1}}{h^2},$$

the error of the numerical scheme being $O(h^2)$.

Ignoring the walkoff terms, Eqs. (1)–(4) can be thus transformed to

$$i\left(\frac{dw_k}{dz}\right)=\mathcal{F}_k, \tag{22}$$

where we further denote

$$w_k\equiv\begin{cases} u_{1k} & \text{for} \quad 1\leqslant k\leqslant n \\ u_{2(k-n)} & \text{for} \quad (n+1)\leqslant k\leqslant 2n \\ v_{1(k-2n)} & \text{for} \quad (2n+1)\leqslant k\leqslant 3n \\ v_{2(k-3n)} & \text{for} \quad (3n+1)\leqslant k\leqslant 4n, \end{cases}$$

and $\mathcal{F}$ is a $1\times 4n$ vector function defined by

$$\mathcal{F}_k=\begin{cases} -\frac{1}{2}\left(\frac{w_{k-1}-2w_k+w_{k+1}}{h^2}\right)+qw_k-w_k^*w_{2n+k}-Qw_{n+k} & \text{for} \quad 1\leqslant k\leqslant n, \\ -\frac{1}{2}\left(\frac{w_{k-1}-2w_k+w_{k+1}}{h^2}\right)+qw_k-w_k^*w_{2n+k}-Qw_{k-n} & \text{for} \quad (n+1)\leqslant k\leqslant 2n, \\ -\frac{1}{4}\left(\frac{w_{k-1}-2w_k+w_{k+1}}{h^2}\right)+\frac{1}{2}w_k-\frac{1}{4}w_{k-2n}^2-\frac{1}{2}Kw_{k+n} & \text{for} \quad (2n+1)\leqslant k\leqslant 3n, \\ -\frac{1}{4}\left(\frac{w_{k-1}-2w_k+w_{k+1}}{h^2}\right)+\frac{1}{2}w_k-\frac{1}{4}w_{k-2n}^2-\frac{1}{2}Kw_{k-n} & \text{for} \quad (3n+1)\leqslant k\leqslant 4n. \end{cases}$$

Of course, the w_{k-1} and w_{k+1} terms have to be equated to zero at the boundaries of the integration domain to get the correct solitary wave solutions.

To find the necessary stationary solutions, we equate the above expressions to zero:

$$\mathcal{F}=0. \tag{23}$$

Again, the Newton-Raphson method is used here to solve Eq. (23). The corresponding Jacobian matrix is obtained by calculating $\partial\mathcal{F}_j/\partial w_k$, where $1\leqslant j\leqslant 4n$, and $1\leqslant k\leqslant 4n$. It is a $4n\times 4n$ matrix. Further technical details on how to obtain the solutions from here onward will not be elaborated on here.

The above-mentioned Jacobian matrix will then also be used for the linear stability analysis, by evaluating its eigenvalues, which is a well-established method, see, e.g., [10] for details. Independent of this, the stability will also be tested directly by means of the split-step Fourier method. The walkoff effects will be investigated by means of the split-step Fourier method too.

III. THE STATIONARY SOLUTIONS

First, we will display results for the stationary solitons obtained by means of VA. We should stress, however, that, except for a peculiar narrow parametric region described below, the variational results are always fairly close to the di-

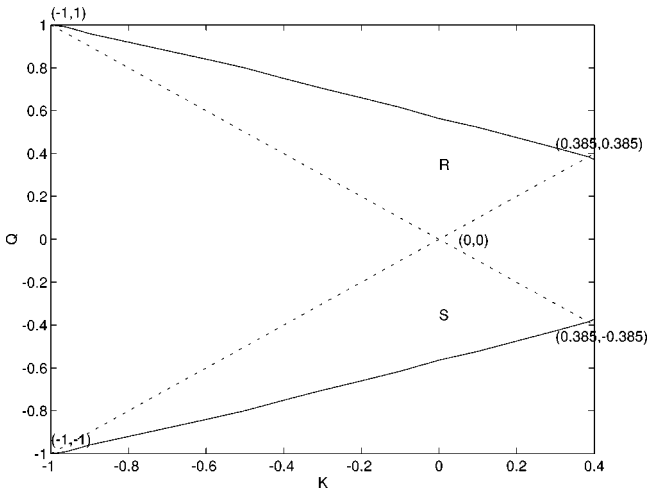

FIG. 1. The bifurcation regions. Asymmetric solitons exist in the regions marked by R and S. The corners of the regions are at $(-1,\pm 1)$, (0,0), and $(0.385,\pm 0.385)$. The dotted lines are the lines $Q=\pm K$, to separate the unphysical area where $|K|>|Q|$. The solid lines are the loci of the bifurcation points found numerically.

rect numerical ones. A detailed comparison will be given at the end of this section. In this and subsequent sections, save Sec. VI, the results will be presented for the case $q=1$.

We have found that the asymmetric soliton solutions exist only in the regions R and S in the (K,Q) plane as shown in Fig. 1. The solid lines mark the loci of the bifurcation points, whereas the dotted lines are $Q=\pm K$, which mark off the physically unrealistic regions where the SH coupling is larger than the FH coupling (i.e., $|K|>|Q|$). Thus, in the two triangular regions delineated by the dotted lines and the vertical axes, the asymmetric solitons do exist, but are physically unrealistic. It is also interesting to note that the range of existence of the asymmetric solitons is found to be

$$-1<K<0.385, \tag{24}$$

which is the same as predicted in [6] (in [6], the upper limit was found exactly as 5/13, which is approximated by 0.385).

It is necessary to mention that there was a serious discrepancy between the analytical (variational) and direct numerical results obtained in [6] for the limit case $K=Q$: while the analytical solution was obtained for the whole interval (24), numerically they had been found only in the subinterval $-0.3<Q<0.385$. In view of the results obtained in the present work, this limitation was produced not by any hidden bifurcations or instability, but solely by technical limitations of the numerical scheme employed in [6].

The variational results allow us to construct two *three-dimensional* bifurcation diagrams shown in Figs. 2 and 3, for FH and SH, respectively. They are plots, versus the coupling constants K and Q, of the effective asymmetry parameters Θ_F and Θ_S defined as follows:

$$\Theta_F=\frac{u_1^2-u_2^2}{u_1^2+u_2^2}, \tag{25}$$

$$\Theta_S=\frac{v_1^2-v_2^2}{v_1^2+v_2^2}, \tag{26}$$

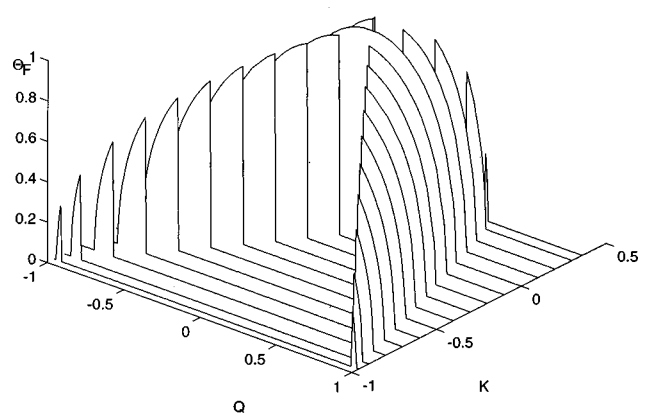

FIG. 2. The bifurcation diagram for the fundamental harmonics. The middle portions are chopped off since $|K|>|Q|$ there.

where $u_{1,2}$ and $v_{1,2}$ without the argument x are the peak values of the corresponding waves. Θ_F and Θ_S are defined to be compatible with the asymmetry parameter $\cos(2\theta)$ that was used in [6]. Note that the middle portions of the curved surfaces, corresponding to the unphysical situation with $|K|>|Q|$, have been eliminated. We stress that, although it is shown in Figs. 2 and 3 that both Θ_F and Θ_S are zero in these regions, asymmetric solitons do exist in these regions as mathematical objects.

In general, at all values of K, the FH fields of the asymmetric solitons are more asymmetric at small $|Q|$. In fact, at $|Q|=|K|=0$, the two waveguides become decoupled, and the field in the second waveguide is absent (we adopt a convention to allocate the number 1 to the waveguide carrying larger fields, i.e., $u_1\geqslant u_2$ and $v_1\geqslant v_2$). As $|Q|$ increases from zero, the asymmetry of the FH fields monotonically decreases; on the other hand, the asymmetry of the SH fields at first gets even stronger, and then rapidly decreases as the bifurcation point is approached. The asymmetric solutions finally merge with the symmetric ones at the bifurcation points. These trends are more evident for more negative K. Close to $K=-1$, the SH fields attain the strongest asymmetry at very sharp parts of the bifurcation diagram (Fig. 3). As K becomes more and more negative, the bifurcation points spread apart towards larger values of $|Q|$.

The characteristics of the asymmetric solutions can be further clarified by looking at Figs. 4 and 5, which are plots

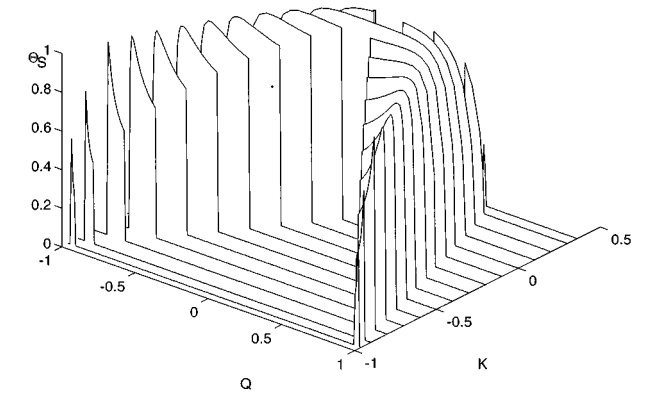

FIG. 3. The bifurcation diagram for the second harmonics. The middle portions are chopped off since $|K|>|Q|$ there.

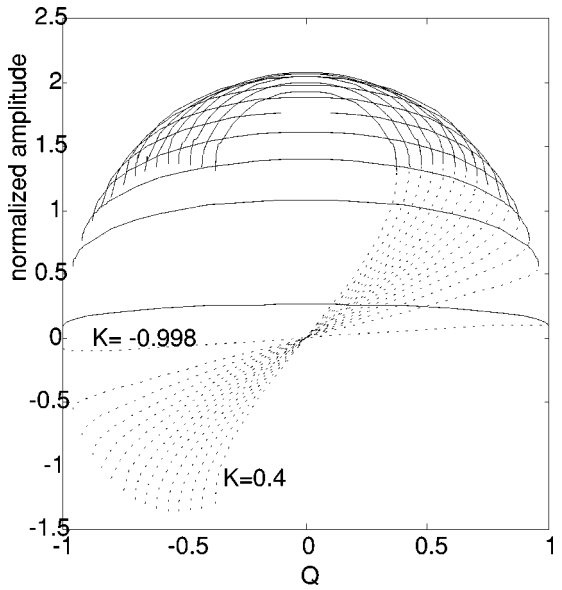

FIG. 4. The peak values of $u_{1,2}$ vs Q, with K fixed as a parameter. The solid lines stand for u_1, and the dotted lines are for u_2. K takes the values: $K=0.4,0.3,\ldots,-0.8,-0.9,-0.998$.

of the peak values of $u_{1,2}$ and $v_{1,2}$ versus Q, with K fixed as a parameter. For both FH and SH fields in the waveguide 1, as K decreases (but remains positive), the fields become larger, and they reach a maximum at $K=0$. Then, as K keeps on decreasing further to negative values, the fields become smaller. The FH field decreases towards zero as $K\rightarrow -1$. In the waveguide 2, both FH and SH decrease as K decreases. We adopt a convention that the amplitudes of the fields in the waveguide 2 are negative when they have the sign opposite to that in the waveguide 1. So, the amplitude of the SH field in the waveguide 2 assumes a larger absolute value when K is getting more negative.

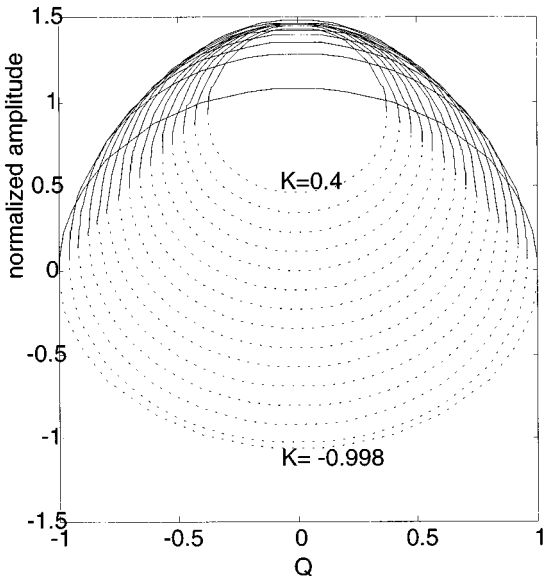

FIG. 5. The peak values of $v_{1,2}$ vs Q, with K fixed as a parameter. The solid lines stand for v_1 and the dotted lines are for v_2. K takes the values $K=0.4,0.3,\ldots,-0.8,-0.9,-0.998$ in this plot.

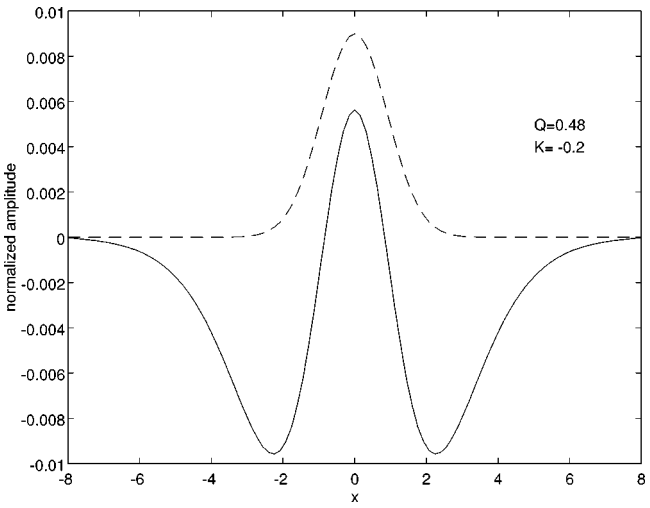

FIG. 6. The shape of the SH component v_2 of the asymmetric soliton at $Q=0.48$ and $K=-0.2$, where the sign reversal of v_2 occurs. The solid line is the actual non-Gaussian shape of the soliton obtained by the modified method of lines. The dashed line is the prediction of the variational approximation. Since the variational approximation uses the Gaussian ansatz, it fails to predict the correct shape in a narrow parametric region around this point.

In fact, at $Q=0$, when $K\rightarrow -1$, the absolute peak values of both v_1 and v_2 approach the same value, but they are of opposite sign, whereas u_1 approaches zero and u_2 is identically zero, so that the soliton becomes antisymmetric, with the dominant SH field. However, since this is an unphysical case, we will not discuss it further.

A noteworthy point is that when K is negative, the field v_2 changes its sign from positive to negative as $|Q|$ decreases past a certain value (depending on the value of K). When this sign reversal takes place, the field v_2 is essentially non-Gaussian over a narrow range of Q, and has a very small value (see Fig. 6). Coincidently, these non-Gaussian solutions correspond to the sharp portions of the strongest asymmetry in the bifurcation diagram for SH (Fig. 3). Thus, VA based on the Gaussian ansatz is inappropriate in this narrow parametric region, but it proves to be appropriate in all the other cases.

The widths of the components of the soliton solutions also vary with K and Q. Figure 7 shows the plot of the spot size versus K and Q for the component u_1, which is defined as follows:

$$W_1=1/\sqrt{\alpha_1}, \tag{27}$$

α_1 being the width parameter according to Eq. (10). In general, the spot size increases towards infinity as $K\rightarrow -1$, $|Q|\rightarrow 1$. As the peak values of the fields are simultaneously approaching zero there, this implies that the solutions are spreading out indefinitely in this limit.

Before proceeding to a comparison of the analytical results obtained by means of VA and numerical findings, it is relevant to mention that, in order to validate our numerical results, we compared them as produced by different methods. As a typical example, we can mention what was obtained for the peak values u_1 of the FH in the waveguide 1. In the limit case $K=Q$, we compared the results obtained

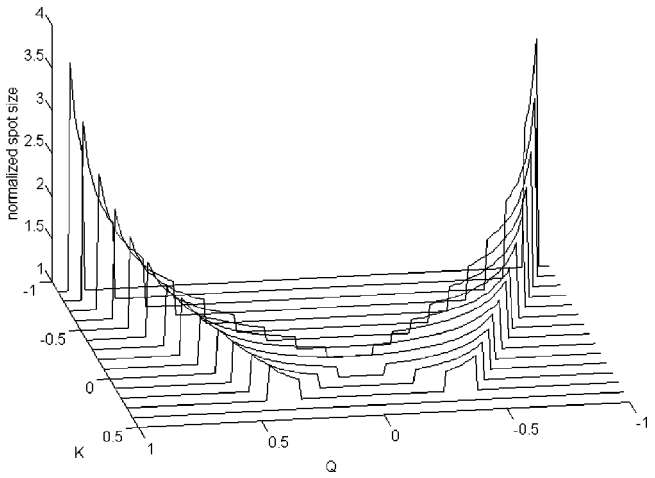

FIG. 7. The spot size of u_1 of asymmetric solitons versus K and Q. The middle portion has been chopped off because $|K|>|Q|$ there. Also, note that the other flat portion of the plot outside the curved surface has no meaning, since data were not gathered for symmetric solitons there.

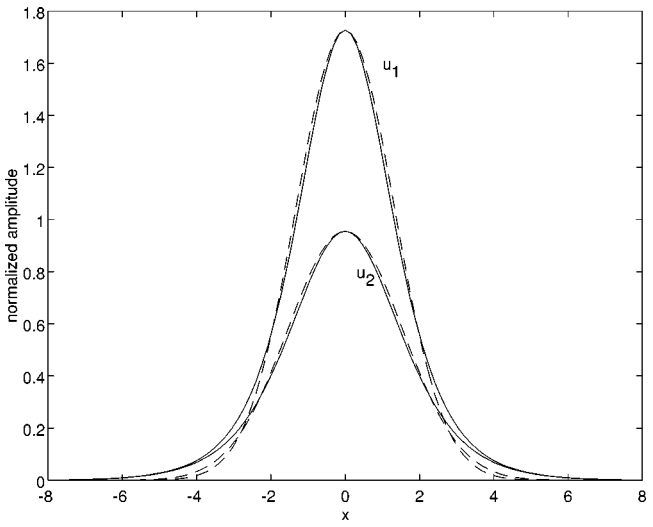

FIG. 8. The shape of the asymmetric soliton at $K=0$, $Q=0.5$. Shown are the FH components $u_{1,2}$. The solid line is the result obtained from the modified method of lines, and the dashed line is generated by the variational approximation.

from the modified method of lines with those produced by the shooting method that was employed previously in [6]. The modified method of lines used 101 lines; i.e., the discrete grid in the x domain has 101 points. The results were compared for the range of Q from -0.2 to 0.3, the worst discrepancy being 1.7% at $Q=-0.2$; otherwise, the discrepancies are all under 1%.

To check the relevance of the results obtained by means of VA, we compared them with those produced by two versions of the modified numerical method of lines, using, respectively, 101 and 161 lines (the latter number was a technical limit set by the computer used), for K and Q taking on different values. In this relation, it is relevant to note, first of all, that the modified methods of lines using, respectively, 101 and 161 lines agree very well with each other, the worst discrepancy being 0.24%. Based on this, we believe that our numerical scheme is reliable.

Comparison between the variational and direct numerical results shows that their differences range from about 2% to about 6%. Generally, the discrepancies are larger very close to the bifurcation points. This is understandable because, as shown in Figs. 2 through 5, the fields change rapidly with Q near these points. Particular results of the comparison are displayed in Table I.

As a typical case, we additionally show in Fig. 8 the shape of the asymmetric soliton at $K=0$ and $Q=0.5$, as obtained from both VA and the modified method of lines. It can be seen that the agreement is very good; the largest deviations are at the skirts of the soliton. The shape produced by VA is narrower there, which is a natural drawback of the Gaussian ansatz. This feature is generic for all the values of K and Q.

IV. THE STABILITY ANALYSIS

In this section, we will study the stability of the stationary solutions found in the previous section. First of all, we can perform a straightforward linear stability analysis, using the Jacobian matrices computed in the process of directly solving the ODE's (5)–(8) by the modified method of lines in the previous section. We use the results of the method based on 101 lines, which means discretizing the variable x at 101 points. The corresponding Jacobian matrices will thus have 404 eigenvalues. If any of these eigenvalues is positive, the stationary solution is regarded to be unstable. Since the calculation of the eigenvalues is straightforward (being a standard feature of the software used), the linear stability was tested for all the stationary solutions found.

Without exception, all the stationary solutions considered (including the symmetric ones) have at least one positive eigenvalue. This, however, does not mean that all the solutions are truly unstable. Indeed, in the conservative system, the stability may be only neutral, implying the existence of at

TABLE I. Sensitivity analysis (discrepancies when compared with method of lines using 161 lines).

	Discrepancies							
K	-0.7		-0.4		0.0		0.3	
Q	0.8	0.874 [a]	0.5	0.725 [a]	0.5	0.56 [a]	0.35	0.425 [a]
ML [b]	0.03%	0.01%	0.06%	0.04%	0.08%	0.09%	0.08%	0.24%
VA [c]	2.9%	5.3%	2.4%	2.9%	2.1%	3.2%	2.3%	5.5%

[a]These columns correspond to points close to the bifurcation points.

[b]Method of lines, using 101 lines.

[c]Variational method.

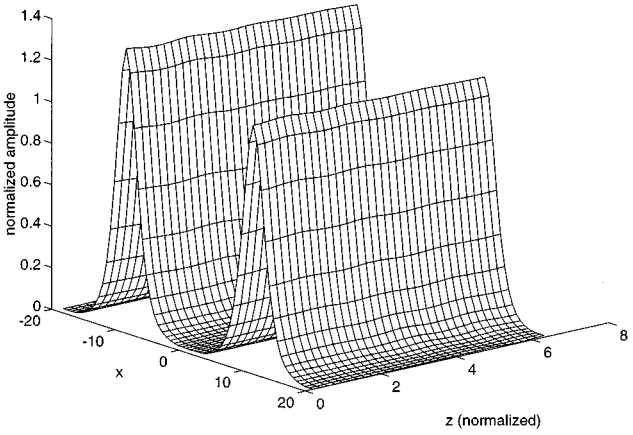

FIG. 9. Evolution of a slightly disturbed asymmetric soliton at $Q=0.7$ and $K=-0.3$. Shown are the fundamental harmonic fields in both waveguides. Distance of propagation simulated was 2π.

least one zero eigenvalue in the linear stability analysis. This fact was, as a matter of fact, observed, for the limit case $K=Q$, in [6] in the form of very persistent, nongrowing and nondecaying, internal vibrations of the asymmetric soliton generated by a small perturbation in the initial conditions. In the numerical computations, however, the zero eigenvalue can easily turn out to be a tiny positive one. On the other hand, this implies that the straightforward numerical calculation of the stability eigenvalues does not provide for the final answer, and direct simulations of the PDE's (1)–(4) with perturbed initial conditions are necessary.

The conventional method of lines, which was used above to produce the stationary soliton solutions, can be used too to solve the PDE's. However, we did not use this method to tackle the stability problem, because, when formulated as above to obtain the stationary solutions, the method turns out to be very inefficient for the PDE integration. Instead, we used the split-step Fourier method as done in [6]. The study of the stability was performed at various points in the parametric space where the asymmetric solitons exist. The selected points were

$$(K,Q)=(-0.3,0.7);(-0.1,-0.4);(0,-0.4);$$

$$(0,-0.56);(0,0.566);(0.2,-0.45);(0.3,0.4).$$

They were chosen so that areas close to and far from the bifurcation points, as well as the regions with positive and negative values of the coupling constants, were all tested.

The results of this analysis are in complete agreement with the inferences formulated in [6]. *All* the asymmetric solitons were found to be neutrally stable. This means that, slightly perturbed, the solitons will undergo minor fluctuations around the stationary solutions over very long distances. The fluctuations do not have any sign of decay, but they are not growing either. This is exactly the same behavior as observed in [6]. A quite typical example of the evolution of a slightly perturbed asymmetric soliton is displayed in Fig. 9, which depicts a case of $Q=0.7$ and $K=-0.3$. This figure displays simultaneously the FH components of the soliton in both waveguides.

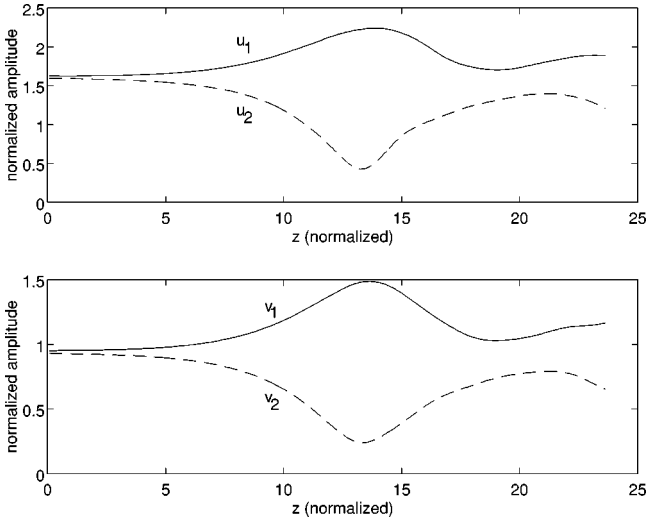

FIG. 10. Evolution of the peak values of the unstable symmetric soliton at $Q=-0.4$, $K=0$. This figure illustrates evolution towards the stable asymmetric soliton.

We also checked stability of the symmetric solitons that coexist with the asymmetric ones. Exactly as expected [6], the symmetric solitons are *always* destabilized by the bifurcation. This is illustrated by Fig. 10. It shows that the unstable symmetric soliton suffers spontaneous symmetry breaking and shows a trend to rearrange itself into a stable asymmetric soliton that exists at the same values of the coupling constants. However, damping of the internal vibrations of the resultant strongly perturbed soliton is so weak that there is no sign of settling down even after a long distance.

V. EFFECTS OF SPATIAL WALKOFF

Because the spatial walkoff is unavoidably present in a real situation, we have also studied its effect by means of the direct PDE simulations, keeping the walkoff terms in Eqs.

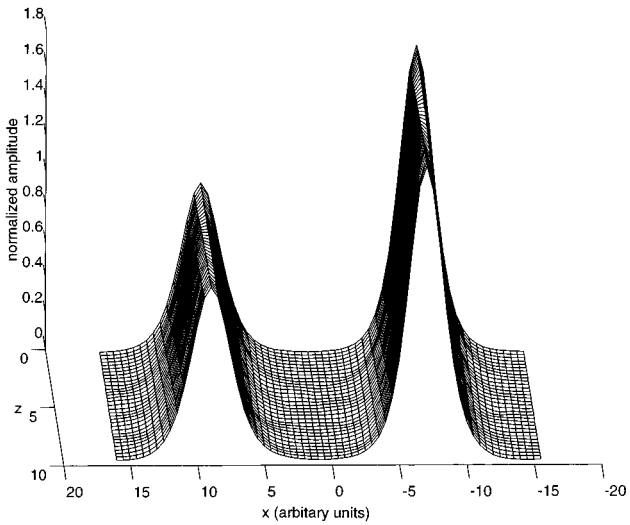

FIG. 11. Evolution of the asymmetric soliton at $Q=0.5$, $K=0$ under the influence of the walkoff effect with $\delta=0.05$. Only the FH components are shown. The slanting propagation directions are due to the walkoff terms. Distance of propagation simulated was 3π.

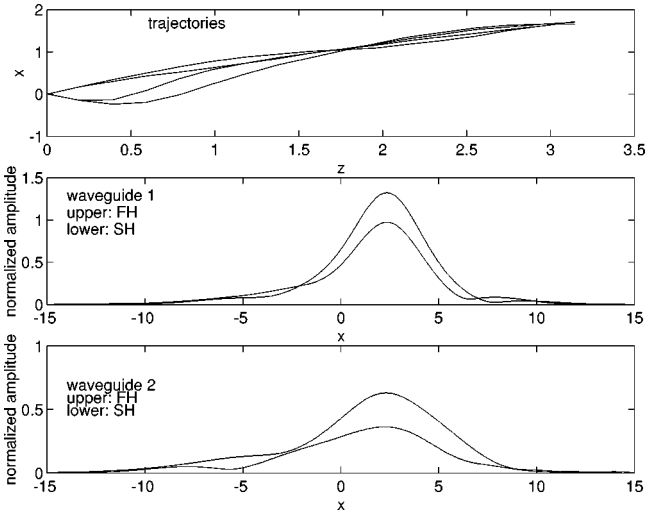

FIG. 12. (a) Trajectories of the peak values of the soliton components. Initially, the upper two traces are those of the FH and SH in waveguide 1, and the lower two traces are those in waveguide 2. It can be noted that they travel in opposite directions. However, the smaller waves in waveguide 2 are finally pulled by the larger waves in waveguide 1 and trapped to follow their direction of travel. (b) The shapes of the soliton components in waveguide 1 and (c) the shapes of the soliton components in waveguide 2, after propagating over a normalized distance of π. In this analysis, $K=Q=-0.7$, $q=1$, and $\delta=0.5$. It can be seen that the walkoff distorts the soliton, making the wave forms to skew to one side.

(1)–(4). Firstly, we demonstrate that the asymmetric solitons are *not* destabilized by the walkoff effect if the walkoff is small enough. In Fig. 11, we illustrate the evolution of an asymmetric soliton under the action of a small walkoff. In this case, $K=0$, $Q=0.5$, and $\delta=0.05$. For typical nonbirefringent group III-V semiconductor crystals, with a refractive index of 3.5, a coherence length of around $10-100$ μm, and a typical wavelength of about 1 μm [11], this corresponds to the actual misalignment of around 0.11–0.34 degrees between the beams in the two waveguides. Actually, available experimental techniques allow one to make the misalignment essentially smaller than this, so these values are quite relevant to estimate limits of the soliton's stability against the walkoff. The total distance of travel simulated was 3π.

In Fig. 12, we illustrate the evolution of another soliton when the walkoff is larger. In this case, $\delta=0.5$, $K=Q=-0.7$. The total distance of travel simulated is π. It can be seen that the shapes of the soliton components get distorted, and skew to one side. It can be also seen that the smaller of the soliton components in the two waveguides gets trapped by the larger soliton component and pulled to travel in the same direction.

In Fig. 13, we summarize the distortion effect inflicted on the soliton as both the walkoff parameter δ and the coupling constants, K and Q are varied (we consider here the case $K=Q$). We quantify the distortion by defining

$$D=\frac{\int_{W_1}|u_1^2-u_{1i}^2|d\zeta}{\int_{W_1}u_{1i}^2 d\zeta}, \tag{28}$$

where the integrations are confined within the beam width (the spot size), W_1, as defined in Eq. (27). u_1 is the FH in waveguide 1 after the propagation distance of π, and u_{1i} is the same wave filed at the input ($z=0$). The integrations are done with respect to the transverse coordinate, ζ, in the reference frame that travels together with u_1.

It can be seen that, in general, the distortion becomes larger as δ gets larger. Also, distortion is larger for larger absolute values of the coupling constants. This trend is very prominent for positive Q: as one sees in Fig. 13, the distor-

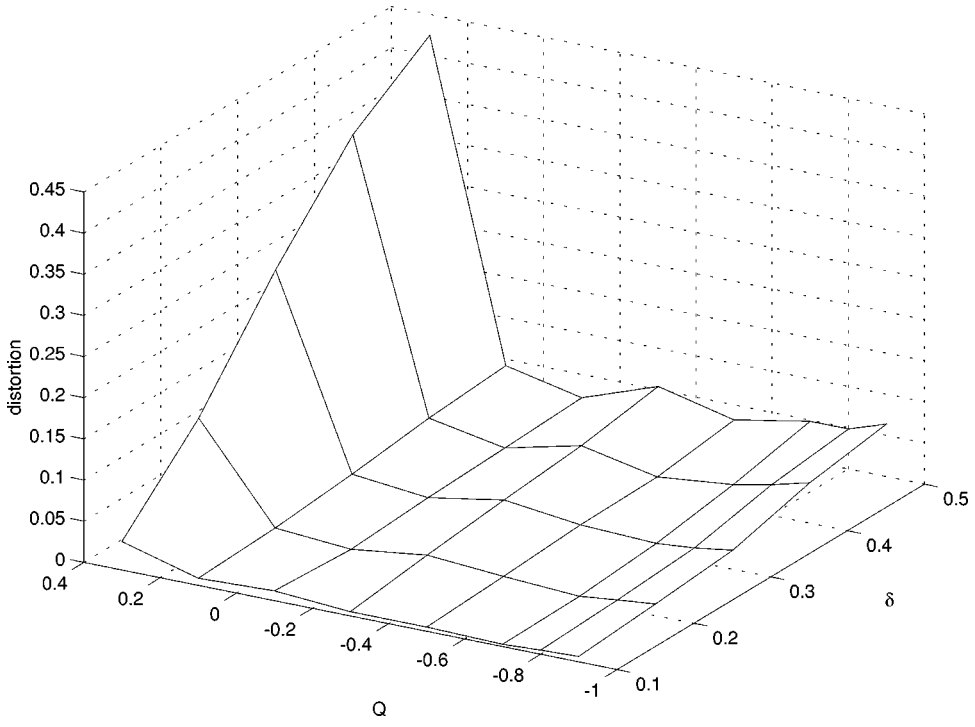

FIG. 13. Distortion as a function of walkoff parameter δ and coupling constant Q. In this analysis, $K=Q$, and distortion is shown after a propagation distance of π. In general, the distortion is larger for larger walkoff, and stronger coupling (where the solitons get more symmetric).

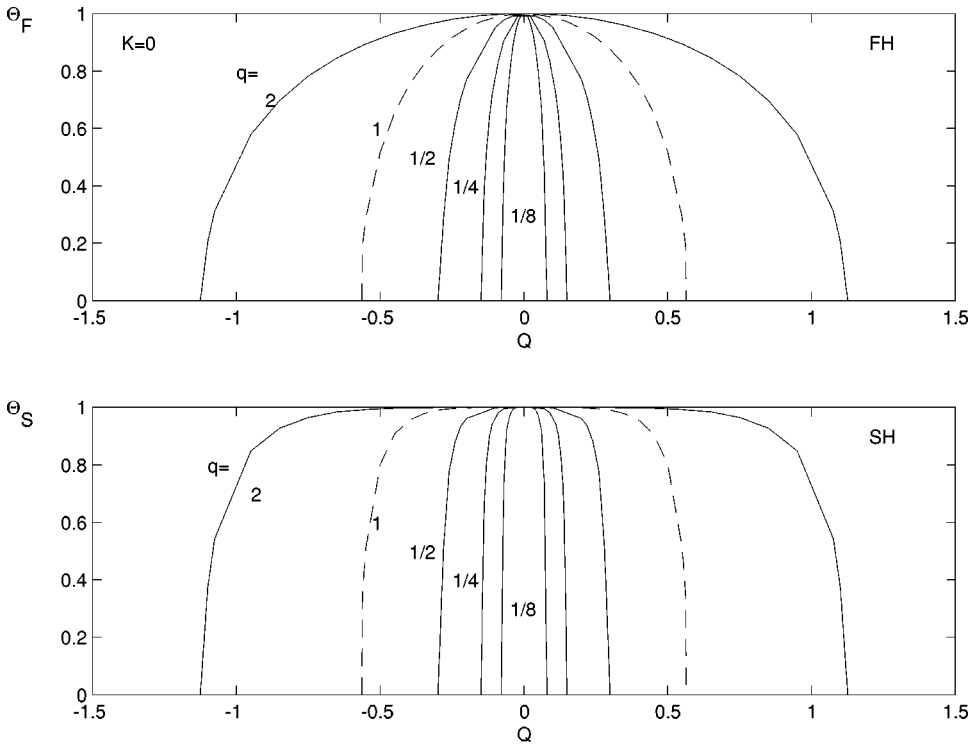

FIG. 14. The asymmetry parameters, $\Theta_{F,S}$, as functions of the fundamental-harmonic coupling constant Q, when the phase mismatch q takes on values 0.125, 0.25, 0.5, 1 and 2. The second-harmonic coupling constant K is fixed at 0. It can be seen that the regions where the asymmetric solitons exist expand as q gets larger. The dashed curves correspond to $q=1$, which are cross sections of the bifurcation diagrams in Figs. 2 and 3.

tion produced by a fixed value of δ steeply increases with the increase of $Q>0$, quickly leading to destruction of the soliton. Because the solitons become more symmetric with the increase of the absolute values of the coupling constants, we can interpret this trend as an effect of pulling apart of two soliton components (referring to the two cores) having nearly equal energies.

We also considered the walkoff-induced deformation of the stable symmetric solitons, existing before the bifurcation. For instance, in the case $K=Q=0.4$, we observed that, in the presence of quite a strong walkoff, $\delta=0.4$, both components of the soliton developed conspicuous side lobes after having traveled a long distance, $z=3\pi$. As walkoff becomes even larger, at $\delta=0.6$, the components in the two cores get pulled apart into the lobes, and they are no longer trapped together to travel in the same direction, which we interpret as destruction of the soliton at some δ between 0.4 and 0.6.

VI. VARYING THE PHASE MISMATCH

Effects produced by varying the mismatch parameter q are practically important, and they turn out to be rather easy to investigate. Running the simulations with different values of q, we have found that, as it gets smaller, the regions where asymmetric solitons can exist shrink; the opposite happens when q gets larger. In fact, as q gets larger, the asymmetry gets larger ($\Theta_{F,S}$ becomes very close to 1) very rapidly. This means the two waveguides get effectively decoupled at a large phase mismatch.

Figure 14 shows the plots of the asymmetry parameters, $\Theta_{F,S}$, versus the FH coupling constant Q for a fixed value of the SH coupling constant K of 0, with the phase mismatch q as a changing parameter, taking on values 0.125, 0.25, 0.5, 1, and 2. Note that the dashed curves, corresponding to $q=1$, are cross sections of the bifurcation diagrams shown in Figs. 2 and 3. Similar analyses had been done for $K=-0.5$ and $K=0.3$. The results are not displayed here as they do not produce anything essentially different. To show the effect of even larger values of q, we include Figs. 15 and 16, for the cases $K=Q$ and $K=0$, respectively, which show that the asymmetry stays relatively constant as q is increased beyond about 4.

The case of very small values of q can be easily considered by means of an approximation well known for the single-core waveguides [2] (one should bear in mind that our parameter q, entering the FH equations, is the inverse of the frequently defined mismatch parameter α in the equation for SH). Namely, one assumes that, in Eqs. (2) and (4), it is possible to neglect all the terms but the last two terms on the left-hand sides, so that SH can be eliminated in favor of FH: $v_n \approx \frac{1}{2}u_n^2$ $(n=1,2)$. Substitution of this into Eqs. (1) and (3) immediately yields a system of two linearly coupled *cubic*

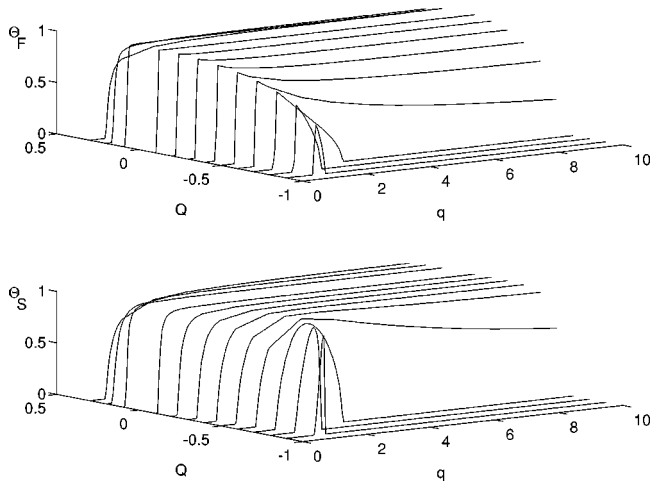

FIG. 15. The bifurcation diagrams as a function of the coupling constant Q and phase mismatch q for the case $K=Q$.

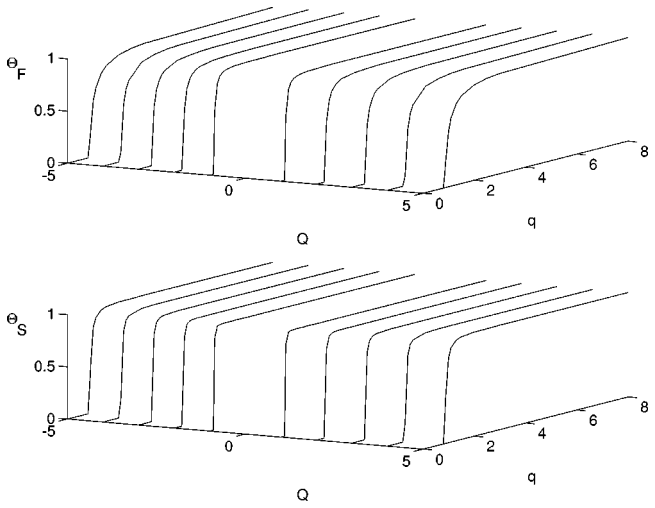

FIG. 16. The bifurcation diagrams as a function of the coupling constant Q and phase mismatch q for the case $K=0$.

nonlinear Schrödinger equations for the FH fields u_n, which is identical to that considered in detail earlier in the context of the twin-core nonlinear optical fibers [7,8].

VII. CONCLUSIONS

In this work, we have presented detailed results for a model of two linearly coupled second-harmonic-generating waveguides. We have studied the general case with different coupling constants for the fundamental and second harmonics. We have completely identified the entire region (that includes two subregions) where the asymmetric solitons exist, along with the bifurcation lines, at which the asymmetric solitons branch off from the obvious symmetric-soliton solutions. The asymmetric solutions were found in two different ways. One (analytical) approach was based on the variational approximation, which used the Gaussian ansatz. As usual, the main advantage of using this type of ansatz is a possibility to admit different components of the soliton to have different widths. Final solutions to the system of eight algebraic equations produced by the variational approximation were found numerically. Another approach was based on direct numerical solution performed in terms of a finite-difference scheme. The agreement between the analytical and direct numerical results turns out to be very good, except for a very narrow region, where the SH component of the soliton is changing its sign, and its shape is strongly non-Gaussian (nonmonotonous).

Then, the stability of these soliton states was tested by direct PDE simulations. The asymmetric solitons, whenever they exist, were shown to be neutrally stable, while the symmetric solitons that obviously coexist with the asymmetric ones are always unstable. Moreover, simulations of evolution of the symmetric solitons close to the bifurcation point and farther from it show that the unstable symmetric solitons suffer spontaneous symmetry breaking and begin to evolve into the corresponding asymmetric solitons (which they do faster if they are farther from the bifurcation point).

We then investigated the effect of the walkoff (spatial misalignment) on the solitons in the coupled waveguides for different values of the coupling constants. An estimate for the values of the walkoff parameter δ corresponding to experimentally relevant values of the misalignment angles was obtained ($\delta \sim 0.05$ for the angles ~ 0.3 deg). The walkoff term being small enough, the asymmetric solitons, as well as the symmetric ones existing before the bifurcation, remain robust. With an increase of the parameter δ, the solitons develop a distortion, and they finally get destroyed when walkoff becomes too large.

Finally, we have also investigated effects produced by varying the phase mismatch parameter. As the phase mismatch parameter q gets smaller than 1, the regions where the asymmetric solitons exist shrink, whereas these regions expand when q gets larger than 1. However, as q increases beyond about 4, the asymmetry stays more or less constant, especially for the case $K=0$. We have also demonstrated that, in the opposite limit of very small q, one can eliminate the second-harmonic fields to transform the model into that for the twin-core fiber with the Kerr nonlinearity.

Thus, the results obtained in this work completely characterize the asymmetric soliton states in the linearly coupled second-harmonic-generating waveguides with arbitrary coupling constants.

[1] Y. N. Karamzin and A. P. Sukhorukov, Zh. Éksp. Teor. Fiz. **68**, 834 (1975) [Sov. Phys. JETP **41**, 414 (1976)].

[2] R. DeSalvo, D. Hagan, M. Sheik-Bahae, G. Stegeman, and E. Van Stryland, Opt. Lett. **17**, 28 (1992); G. Assanto, G. Stegeman, M. Sheik-Bahae, and E. Van Stryland, Appl. Phys. Lett. **62**, 1323 (1993); R. Schiek, J. Opt. Soc. Am. B **10**, 1848 (1993); M. J. Werner and P. D. Drummond, *ibid.* **10**, 2390 (1993); A. V. Buryak and Yu. S. Kivshar, Opt. Lett. **19**, 1612 (1994); Phys. Lett. A **197**, 407 (1995); L. Turner, C. M. Menyuk, and G. I. Stegeman, Opt. Lett. **19**, 1615 (1994); J. Opt. Soc. Am. B **12**, 889 (1995); W. E. Torruellas, Z. Wang, D. J. Hagan, E. W. Van Stryland, G. I. Stegeman, I. Torner, and C. R. Menyuk, Phys. Rev. Lett. **74**, 5036 (1995); R. Schiek, Y. Baek, and G. I. Stegeman, Phys. Rev. E **53**, 1138 (1996); D. E. Pelinovsky, A. V. Buryak, and Yu. S. Kivshar, Phys. Rev. Lett. **75**, 591 (1995); A. V. Buryak, Yu. S. Kivshar, and V. V. Steblina, Phys. Rev. A **52**, 1670 (1995); S. Trillo and P. Ferro, Opt. Lett. **20**, 438 (1995); P. Drummond, H. He, and B. A. Malomed, Opt. Commun. **123**, 394 (1996); C. Etrich, T. Peschel, F. Lederer, B. A. Malomed, and Y. S. Kivshar, Phys. Rev. E **54**, 4321 (1996); H. He, M. J. Werner, and P. D. Drummond, *ibid.* **54**, 896 (1996); L. Torner, D. Mazilu, and D. Mihalache, Phys. Rev. Lett. **77**, 2455 (1996).

[3] V. Steblina, Y. S. Kivshar, M. Lisak, and b. A. Malomed, Opt. Commun. **118**, 345 (1995).

[4] G. Assanto, G. Stegeman, M. Sheik-Bahae, and E. Van Stryland, Appl. Phys. Lett. **62**, 1323 (1993); G. Assanto, A. Laureti-Palma, C. Sibilia, and M. Bertolotti, Opt. Commun. **110**, 599 (1994).

[5] M. A. Karpierz, in, *Nonlinear Guided Waves and Their Appli-*

cations, OSA 1996 Technical Digest Series (Optical Society of America, Washington D.C., 1996), Vol. 15, p. 70.

[6] W. C. K. Mak, B. A. Malomed, and P. L. Chu, Phys. Rev. E **55**, 6134 (1997).

[7] N. Akhmediev and J. M. Soto-Crespo, Phys. Rev. E **49**, 4519 (1994).

[8] B. A. Malomed, I. M. Skinner, P. L. Chu, and G. D. Peng, Phys. Rev. E **53**, 4084 (1996).

[9] J. R. Rice, *Numerical Methods, Software, and Analysis* (McGraw-Hill, New York, 1983), Chap. 7.

[10] R. Seydel, *From Equilibrium to Chaos: Practical Bifurcation and Stability Analysis* (Elsevier Science Publishing, New York, 1988), Chap. 1.

[11] P. N. Butcher and D. Cotter, *The Elements of Nonlinear Optics* (Cambridge University Press, Cambridge, Great Britain, 1990), pp. 222 and 308.